



RESEARCH ARTICLE | JULY 25 2025

Ring polymer molecular dynamics with independent-bead approximation

Special Collection: [Annabella Selloni Festschrift](#)

Ruji Zhao  ; Sheng Meng  



J. Chem. Phys. 163, 044112 (2025)

<https://doi.org/10.1063/5.0283428>



Articles You May Be Interested In

Non-adiabatic ring polymer molecular dynamics in the phase space of the $SU(N)$ Lie group

J. Chem. Phys. (January 2023)

Analysis of variants of non-adiabatic ring polymer molecular dynamics for calculating excited state dynamics

J. Chem. Phys. (May 2025)

State dependent ring polymer molecular dynamics for investigating excited nonadiabatic dynamics

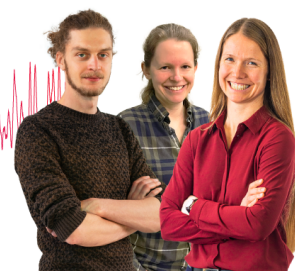
J. Chem. Phys. (June 2019)

Webinar From Noise to Knowledge

May 13th – Register now



Universität
Konstanz



Ring polymer molecular dynamics with independent-bead approximation

Cite as: J. Chem. Phys. 163, 044112 (2025); doi: 10.1063/5.0283428

Submitted: 31 May 2025 • Accepted: 3 July 2025 •

Published Online: 25 July 2025



View Online



Export Citation



CrossMark

Ruji Zhao^{1,2} and Sheng Meng^{1,2,3,a)}

AFFILIATIONS

¹ Beijing National Laboratory for Condensed Matter Physics and Institute of Physics, Chinese Academy of Sciences, Beijing 100190, China

² School of Physical Sciences, University of Chinese Academy of Sciences, Beijing 100049, China

³ Songshan Lake Materials Laboratory, Dongguan, Guangdong 523808, China

Note: This paper is part of the JCP Special Topic, Annabella Selloni Festschrift.

a) Author to whom correspondence should be addressed: smeng@iphy.ac.cn

ABSTRACT

It was recently reported [Zhao *et al.*, Phys. Rev. Lett. **130**, 166401 (2023)] that the full quantum dynamics of a correlated electron–nuclear system can be approximated to the dynamics of a classical ring polymer isomorphism with n beads each bearing distinct electronic configurations, namely, ring polymer molecular dynamics with independent-bead approximation. Here, we present a detailed description of the formalism, including the idea of this approximation and how it combines with existing Ehrenfest dynamics. This approach is applied to several model systems and compared with exact full quantum wavepacket dynamics, along with the widely used fewest switch surface hopping and standard Ehrenfest mean-field dynamics. The evolution of real-time electronic population and quantum nuclear trajectories obtained by this approach is in good agreement with the exact quantum solution, even in regions of strong non-adiabatic coupling, where the conventional surface hopping and Ehrenfest approaches fail to yield adequate results.

Published under an exclusive license by AIP Publishing. <https://doi.org/10.1063/5.0283428>

I. INTRODUCTION

The accurate numerical solution to the full quantum dynamics poses a considerable challenge in materials science and condensed matter physics, including the description of electron–nuclear interaction and multi-electronic states. Solving the time-dependent Schrödinger equation in its full dimension would be the most straightforward way to deal with the coupled electron–nuclear system, but the computational cost scales exponentially with the system's degrees of freedom. Therefore, it is limited to small systems, including only a few electrons and nuclei. There exist several strategies to deal with this problem: One is to simplify the Hamiltonian, neglecting the coupling between electronic and nuclear degrees of freedom, namely, the Born–Oppenheimer adiabatic approximation.¹ The Born–Oppenheimer approximation assumes that the nuclear wavepacket is propagated on a single potential energy surface (PES) determined by the ground state of the electronic subsystem. However, when the PES of different electronic states cross or get close to each other, the strength of non-adiabatic

coupling (NAC) between them cannot be neglected, leading to the breakdown of the Born–Oppenheimer approximation and electronic transitions between different electronic states.^{2–4} Another way is to simplify the nuclear wavefunction. For example, the mixed quantum–classical (MQC)^{5–8} methods treat the electrons as a quantum system evolving according to the Schrödinger equation and the nuclei as classical particles following the Newtonian equation. The widely used mixed quantum–classical methods include Ehrenfest dynamics⁹ (where the nuclei move on the mean-field PES of electronic states) and surface hopping¹⁰ (where the nuclear motion is replaced by a swarm of trajectories moving on and hopping between different electronic states), which are successfully applied to a variety of fields, such as light-induced phase transition,^{11,12} proton transfer,^{13,14} and photochemical reactions.^{15,16} However, therein the nuclei are still regarded as classical particles and lose their intrinsic quantum nature, ignoring nuclear quantum effects (NQE), such as nuclear quantum tunneling and zero-point energy, which can play indispensable roles in systems containing light elements and at low temperatures.

Approximations have to be made to take account of the interplay between the quantized nuclei and electrons in realistic systems. Existing methods have been proposed to incorporate nuclear quantum effects in the non-adiabatic simulations, such as multi-configuration time-dependent Hartree (MCTDH),^{17,18} variational multi-configuration Gaussian (vMCG),¹⁹ and exact factorization.^{20,21} Nonetheless, these methods require propagation of the nuclear wavefunction and, therefore, still suffer from heavy computational complexity. Approximate approaches that treat quantized electron-ion correlations in condensed matter with feasible computational cost are urgently needed and of special practical interest.

The path integral molecular dynamics (PIMD),^{22,23} based on Feynman's path integral theory,²⁴ begins to enter the mainstream due to its computational simplicity. The quantum Boltzmann distribution of a nucleus can be mapped onto a classical ring polymer system, and thus, the quantum mechanical effects of the nucleus are connected to the classical statistical properties of the hypothetical ring of particles based on this isomorphism.^{25,26} There are several simulation techniques using PIMD formulation to incorporate NQEs, including the centroid molecular dynamics (CMD)^{27–29} and ring polymer molecular dynamics (RPMD).^{30,31} CMD propagates classical trajectories in an effective potential surface generated by thermal fluctuations of the ring polymer around its centroid, and RPMD is a classical MD in the extended ring polymer phase space. These PIMD and PIMD-based methods have been successfully applied to treat aspects including NQEs, such as in quantum paraelectric materials^{32,33} and metallic hydrogen.^{34–37} Nonetheless, the standard PIMD approaches are confined to adiabatic MD, and thus, it is still a big challenge to incorporate non-adiabatic effects in path-integral-based MD. To this end, modified RPMD approaches have been proposed: the RPMD can be combined with the surface hopping algorithm, such as RPMD with surface hopping (RPSH),³⁸ and ring polymer surface hopping in isomorphic Hamiltonian (SH-RP-iso).³⁹ An alternative way is to transform the discrete electronic states into continuous variables for computational tractability, such as nonadiabatic RPMD (NRPM), which maps the electronic levels onto a set of harmonic oscillator eigenstates,⁴⁰ the coherent state mapping RPMD (CS-RPMD) using coherent states instead,⁴¹ and spin mapping NRPM (SM-NRPM), which employs spin coherent basis for two-level systems and generators of the SU(N) Lie algebra for more electronic states.⁴² However, the quantum electron-nuclear interaction induces an extra heavy computational cost. In addition, most methods employ the diabatic representation and, therefore, are challenging for practical calculations of real materials. A promising way to deal with the diabatic representation is to use the quasi-diabatic (QD) representation,^{43,44} which can be combined with NRPM theoretically. However, the systematic implementation of the QD propagation scheme in complex condensed matter systems is yet lacking. There is an urgent need to develop a novel computational approach capable of handling realistic large-scale molecular and materials systems while maintaining quantum mechanical accuracy comparable to exact solutions. An algorithm that can be implemented in the framework of the state-of-the-art real time time-dependent density functional theory (TDDFT) is a promising way in this regard.

We recently proposed a new approach that incorporates multiple electronic states in RPMD, dubbed the independent-bead (IB)

approximation.⁴⁵ This method extends RPMD to take into account nonadiabatic electronic transitions in such a way: each bead is regarded as a sample of a nucleus in the quantum configuration space and evolves on the independent effective potential energy surface generated *on the fly*. We have shown that this approach yields excellent agreement with the experimental results in the case of light-induced proton transfer in H₂O-H₂O⁺ as compared to the standard Ehrenfest calculations. To further validate the accuracy of this approach, a systematic comparison between PRMD-IB and other mixed quantum-classical methods is desirable.

In this work, we apply the RPMD-IB scheme in several one-dimensional, two-state model systems. Compared with other methods, namely, conventional Ehrenfest dynamics and fewest switch surface hopping (FSSH) simulations, the presented scheme can provide the most accurate description of electronic transition as well as nuclear quantum trajectories against the exact quantum solutions. We also artificially increase the NAC strength between the two electronic states and find that the real-time electronic population in standard Ehrenfest and FSSH approaches severely deviates from the exact wavepacket results, while our RPMD-IB shows good agreement with the quantum mechanical solution.

This paper is organized as follows: we give a brief review of full quantum dynamics in Sec. II; the mixed quantum-classical dynamics, namely, Ehrenfest and FSSH dynamics, are discussed in Sec. III. In Sec. IV, the main features and assumptions of the new approach are presented. The new method is applied to the model systems, and the performance is tested against accurate quantum-mechanical results in Sec. V.

II. FULL QUANTUM DYNAMICS

For simplicity, we consider the system with a single nuclear degree of freedom with mass M . The generalization to two or three dimensions and more nuclei with different masses is straightforward.

The total Hamiltonian for the coupled electron-nuclear system is

$$\hat{H}(r, R) = \hat{T}_N + \hat{H}_{el}(r, R), \quad (1)$$

where r designates the collection of electronic coordinates and R stands for the nuclear position. \hat{T}_N is the nuclear kinetic Hamiltonian, and \hat{H}_{el} represents the electronic Hamiltonian operator at the fixed nuclear position.

We can use the adiabatic basis to describe electronic states by the following equation:

$$\hat{H}_{el}(r, R)\varphi_i(r, R) = E_i(R)\varphi_i(r, R). \quad (2)$$

The eigenfunctions $\varphi_i(r, R)$ constitute the adiabatic basis, and $E_i(R)$ is the corresponding adiabatic potential energy for each state i , respectively.

With the Born-Huang expansion,⁴⁶ the coupled electron-nuclear wavefunction $\Psi(r, R, t)$ can be expanded in the adiabatic basis as

$$\Psi(r, R, t) = \sum_i \chi_i(R, t)\varphi_i(r, R). \quad (3)$$

The expansion coefficients $\chi_i(R, t)$ represent the nuclear wavefunction at the i th state.

Inserting Eq. (3) into the time-dependent Schrödinger equation,

$$i\hbar \frac{\partial}{\partial t} \Psi(r, R, t) = \hat{H} \Psi(r, R, t), \quad (4)$$

multiplied by $\varphi_i^*(r, R)$, and integrating over all electronic degrees of freedom r , we have the evolution equation of the nuclear wavefunction,

$$i\hbar \frac{\partial}{\partial t} \chi_i(R, t) = \left[-\frac{\hbar^2}{2M} \nabla^2 + E_i(R) \right] \chi_i(R, t) + \sum_j C_{ij}(R) \chi_j(R, t), \quad (5)$$

where $C_{ij}(R)$ is the non-adiabatic coupling (NAC) matrix element, including the first-order coupling vector $d_{ij}(R)$ and second-order coupling scalar $D_{ij}(R)$,

$$C_{ij}(R) = -\frac{\hbar^2}{2M} D_{ij}(R) + \frac{\hbar^2}{M} d_{ij}(R) \nabla_R, \quad (6)$$

with

$$D_{ij}(R) = \langle \varphi_i(r, R) | \nabla_R^2 | \varphi_j(r, R) \rangle_r \quad (7)$$

and

$$d_{ij}(R) = \langle \varphi_i(r, R) | \nabla_R | \varphi_j(r, R) \rangle_r. \quad (8)$$

The brackets $\langle \dots | \dots \rangle_r$ here indicate the integral over electronic degrees of freedom only. When the nuclear wavepacket enters the NAC region, a part of the wavepacket would split into other potential energy surfaces according to Eq. (5), resulting in the non-adiabatic transition between different electronic states, as shown in Fig. 1. As the NAC strength approaches zero and is neglected, the non-adiabatic dynamics fits well with the framework of the Born–Oppenheimer approximation, and the nuclear wavepacket is only propagated on a single ground-state energy surface.

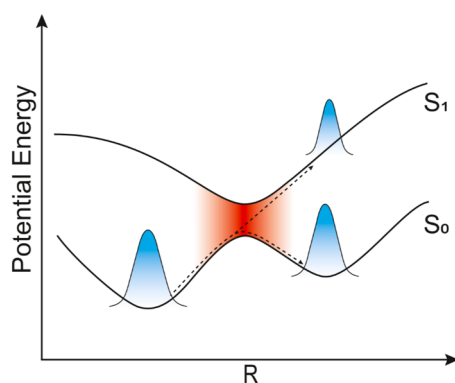


FIG. 1. Schematic diagram of non-adiabatic processes. S_0 and S_1 are two adiabatic potential energy surfaces; the red region denotes the non-adiabatic coupling strength. R represents the nuclear coordinate. When a nuclear wavepacket enters the strong non-adiabatic coupling region, a part of the wavepacket would split into the upper potential energy surface, indicating the occurrence of non-adiabatic transition.

III. MIXED QUANTUM-CLASSICAL DYNAMICS

Since the numerical propagation of nuclear wavefunction requires heavy computational cost, it is a common strategy to approximate the quantized nuclear subsystem with particular spatial and momentum distributions by classical particles while still treating the electronic subsystem quantum mechanically. In trajectory-based MQC methods, the evolution of the electronic wavefunction is solved by propagating the time-dependent Schrödinger equation of the electronic subsystem, and the nucleus can move on the mean-field potential energy surface generated by the electronic states, which leads to the Ehrenfest dynamics, or it can be described by a swarm of trajectories that move on and hop between different PESs, which produces the idea of surface hopping.

A. Ehrenfest dynamics

In the Ehrenfest dynamics, the nucleus moves along an “effective” classical trajectory, and therefore, the electronic Hamiltonian becomes parametrically dependent on time through this nuclear trajectory. The electronic wavefunction $\Phi(r, R, t)$ can be expanded on the adiabatic bases as

$$\Phi(r, R, t) = \sum_i c_i(t) \varphi_i(r, R), \quad (9)$$

where $c_i(t)$ are the time-dependent complex coefficients. The time-dependent Schrödinger equation for the electronic subsystem then becomes

$$i\hbar \dot{c}_i = E_i(R) c_i - i\hbar \sum_j \dot{R} \cdot d_{ij}(R) c_j. \quad (10)$$

The second term on the right-hand side (rhs) of Eq. (10) is responsible for the non-adiabatic transition between different adiabatic states.

The equation of motion for the nuclear trajectory can be obtained by the time-dependent self-consistent field method,⁴⁷ which gives

$$M\ddot{R}(t) = \int \Phi^*(r, R, t) [-\nabla_R \hat{H}_{el}(r, R)] \Phi(r, R, t) dr. \quad (11)$$

Inserting Eqs. (9) and (10) into Eq. (11), we have

$$M\ddot{R}(t) = -\sum_i |c_i|^2 [\nabla_R E_i(R)] + \sum_{i \neq j} c_i^* c_j [E_i(R) - E_j(R)] d_{ij}(R). \quad (12)$$

The first term on the rhs of Eq. (12) represents the weighted averaged force over all adiabatic PESs, and the second term denotes the contribution of the off-diagonal term of the density matrix.

In Ehrenfest dynamics, Eqs. (10) and (12) are solved self-consistently, making the nucleus move on the mean-field potential generated *on-the-fly*.

B. Fewest switch surface hopping

In the fewest switch surface hopping method, the motion of nuclei is represented by a swarm of classical trajectories.¹⁰ The evolution of electronic states follows Eq. (10) for each trajectory, and each trajectory moves on a single potential energy surface except for instantaneous jump under certain conditions.

The probability for hopping from the current state i to some other state j during the time interval t to $t + \delta t$ is

$$p_{ij}(t, \delta t) = \frac{2 \operatorname{Re}[c_i^* c_j d_{ij}(R) \cdot \dot{R}] \delta t}{|c_i|^2}. \quad (13)$$

If the hopping probability p_{ij} is negative, then it is set to zero. One can generate a uniform random number ξ between zero and one. If ξ satisfies the condition

$$\sum_{l=1, l \neq i}^{j-1} p_{il} < \xi < \sum_{l=1, l \neq i}^j p_{il}, \quad (14)$$

the hop from state i to state j would occur, and the trajectory begins to evolve on the E_j state with the adjusted nuclear momentum parallel to the non-adiabatic coupling vector to conserve the total energy. When the required momentum reduction is greater than the kinetic energy along the direction of the non-adiabatic coupling vector, the hop is rejected and considered as a frustrated hop, and the trajectory stays on the current PES.

The hopping algorithm from Eqs. (13) and (14) ensures that except for the frustrated hops, the proportion of trajectories on a given state equals the quantum population $|c_i|^2$ at any time t . If the frustrated hop happens, this consistency is not satisfied anymore.

Both the Ehrenfest dynamics and surface hopping algorithm are effective methods to incorporate the non-adiabatic effects into the dynamics of the electron–nuclear system, but they lack the description of quantized nuclei, which leads to the “over coherence” problem and inadequate results in the strong non-adiabatic region, as we shall demonstrate in Sec. V.

IV. RING POLYMER MOLECULAR DYNAMICS WITH INDEPENDENT-BEAD APPROXIMATION

In this section, we aim to develop an approximate approach to the full quantum non-adiabatic dynamics. The traditional RPMD method, which takes NQEs into account in the framework of the Born–Oppenheimer approximation, is extended to incorporate non-adiabatic electronic transitions via Ehrenfest-like dynamics. We present a detailed description of this RPMD-IB approach starting from the ring polymer isomorphous Hamiltonian in the non-adiabatic electron–nuclear systems.⁴⁵

The quantum canonical partition function of the system is

$$Z = \operatorname{Tr}_{el} \operatorname{Tr}_{nu} [e^{-\beta \hat{H}}] = \lim_{n \rightarrow \infty} \operatorname{Tr}_{el} \operatorname{Tr}_{nu} [(e^{-\beta \hat{H}})^n], \quad (15)$$

where Tr_{el} and Tr_{nu} indicate the trace over electronic and nuclear degrees of freedom, respectively. β is the inverse temperature $1/k_B T$, where k_B is the Boltzmann constant and $\beta_n = \beta/n$.

The trace can be evaluated by integrating over the nuclear position R_1 and summing over the electronic adiabatic basis s_1 ,

$$Z_n \equiv \operatorname{Tr}_{el} \operatorname{Tr}_{nu} [(e^{-\beta_n \hat{H}})^n] = \int dR_1 \sum_{s_1} \langle R_1 s_1 | (e^{-\beta_n \hat{H}})^n | R_1 s_1 \rangle. \quad (16)$$

According to the short-time approximation,⁴⁸ $e^{-\beta_n \hat{H}} \approx e^{-\beta_n \hat{H}_{el}} e^{-\beta_n \hat{T}_N}$ and inserting the unit operator $\hat{1} = \int dR_k \sum_{s_k} |R_k s_k\rangle \langle R_k s_k|$ between each $e^{-\beta_n \hat{H}_{el}} e^{-\beta_n \hat{T}_N}$ term, and note that

$$\langle R_s | e^{-\beta_n \hat{H}_{el}} e^{-\beta_n \hat{T}_N} | R' s' \rangle = \langle s | e^{-\beta_n \hat{H}_{el}(R)} | s' \rangle \langle R | e^{-\beta_n \hat{T}_N} | R' \rangle. \quad (17)$$

For the second term on the rhs of Eq. (17), we have

$$\begin{aligned} \langle R_k | e^{-\beta_n \hat{T}_N} | R_{k+1} \rangle &= \int dP_k \langle R_k | e^{-\beta_n \hat{T}_N} | P_k \rangle \langle P_k | R_{k+1} \rangle \\ &= \int dP_k e^{-\frac{\beta_n P_k^2}{2M}} \langle R_k | P_k \rangle \langle P_k | R_{k+1} \rangle \\ &= \frac{1}{2\pi\hbar} \sqrt{\frac{2\pi M}{\beta_n}} e^{-\frac{\beta_n M}{2\beta_n^2 \hbar^2} (R_k - R_{k+1})^2} \\ &= \frac{1}{2\pi\hbar} \int dP_k e^{-\beta_n \left[\frac{P_k^2}{2M} + \frac{M}{2\beta_n^2 \hbar^2} (R_k - R_{k+1})^2 \right]}, \end{aligned} \quad (18)$$

and therefore, the partition function becomes

$$Z_n = \frac{1}{(2\pi\hbar)^n} \int d\mathbf{P} \int d\mathbf{R} \operatorname{sgn}[\Gamma(\mathbf{R})] e^{-\beta_n H_n(\mathbf{P}, \mathbf{R})}, \quad (19)$$

where the Hamiltonian is

$$H_n(\mathbf{P}, \mathbf{R}) = \sum_{k=1}^n \left[\frac{P_k^2}{2M} + \frac{1}{2} M \omega_n^2 (R_k - R_{k+1})^2 \right] + V(\mathbf{R}). \quad (20)$$

\mathbf{P} and \mathbf{R} are the collective variables of momentum and position for $k = 1, \dots, n$. The cyclic boundary subject to $R_{n+1} = R_1$ is used, and $\omega_n = 1/\beta_n \hbar$. Therefore, the quantized nucleus is mapped to a ring polymer isomorphism composed of n “beads,” where P_k represents the momentum of the k th bead. All beads move on the non-adiabatic potential,

$$V(\mathbf{R}) = -\frac{1}{\beta_n} \ln |\Gamma(\mathbf{R})|, \quad (21a)$$

with

$$\Gamma(\mathbf{R}) = \sum_{s_1} \dots \sum_{s_n} \langle s_1 | e^{-\beta_n \hat{H}_{el}(R_1)} | s_2 \rangle \dots \langle s_n | e^{-\beta_n \hat{H}_{el}(R_n)} | s_1 \rangle, \quad (21b)$$

where each $s_k \equiv s_k(R_k)$ runs over a complete basis set $\{\varphi_1(r, R_k), \dots, \varphi_m(r, R_k)\}$. The sign function in Eq. (19) is necessary since $\Gamma(\mathbf{R})$ sometimes can take on small negative values.⁴⁹ A similar expression to Eq. (21a) has been derived by Schwieters and Voth⁵⁰ although it was used to calculate the transition rate in the path-integral quantum transition-state theory and not for the evolution of real-time dynamics. The potential $V(\mathbf{R})$ is a function of the positions of all beads, and the dynamics generated from this effective potential presents an outstanding computational challenge, especially in the framework of first principles calculations of real materials, and will not, in general, recover the quantum equilibrium distribution. To make the potential computationally feasible, an approximation to Eq. (21a) is needed.

Schmidt and Tully⁴⁹ pointed out that the beads would move on the thermally averaged mean-field potential in the equilibrium case. Here, we extend this idea to the ultrafast dynamics when the system is evolved in the non-equilibrium state, and suppose that each bead bears a distinct electronic configuration and moves on the dynamical mean-field potential according to their respective electronic wavefunction $\Phi(r, R_k, t)$. In practice, the dynamical mean-field can be obtained from the Ehrenfest theorem. Therefore, the complicated

potential $\underline{V}(\mathbf{R})$ could be replaced by the summation of all beads' effective potential energy,

$$\underline{V}(\mathbf{R}) \rightarrow \sum_{k=1}^n V_{\text{eff}}(R_k, t) = \sum_{k=1}^n \langle \Phi_{el}(r, R_k, t) | \hat{H}_{el} | \Phi_{el}(r, R_k, t) \rangle. \quad (22)$$

Note that the effective potential now explicitly depends on time. The Hamiltonian of the ring polymer system with n beads then becomes

$$H_n^{IB}(\mathbf{P}, \mathbf{R}) = \sum_{k=1}^n \left[\frac{P_k^2}{2M} + \frac{1}{2} M \omega_n^2 (R_k - R_{k+1})^2 + V_{\text{eff}}(R_k, t) \right]. \quad (23)$$

The approximated Hamiltonian in Eq. (23) generates the equations of motion,

$$\dot{P}_k = -\frac{M}{\beta_n^2 \hbar^2} (2R_k - R_{k+1} - R_{k-1}) - \frac{\partial V_{\text{eff}}(R_k, t)}{\partial R_k} \quad (24)$$

and

$$\dot{R}_k = \frac{P_k}{M} \quad (25)$$

for $k = 1, \dots, n$. The evolution of the electronic wavefunction for each bead is then given by

$$i\hbar \dot{c}_{i,k} = E_i(R_k) c_{i,k} - i\hbar \sum_j \dot{R}_k \cdot d_{ij}(R_k) c_{j,k}. \quad (26)$$

The dynamical property of the system can be obtained by propagating each bead according to Eqs. (24)–(26) self-consistently. The spring constant $M\omega_n^2$ for the isomorphism ring polymer is proportional to $(nk_B T)^2$, and in the high temperature limit, the ring polymer system would collapse into a single classical particle because of the too stiff spring constant.

V. COMPARISON WITH EXACT QUANTUM CALCULATION

The RPMD-IB takes a bold approximation to $\underline{V}(\mathbf{R})$ in Eq. (22). We have verified in the previous work⁴⁵ the accuracy of RPMD-IB as compared to RPMD with the centroid approximation and bead approximation,³⁸ which can be directly implemented in the TDDFT algorithm, but the systematic comparison with Ehrenfest dynamics and FSSH is lacking. To further validate the accuracy of this approach, we apply this RPMD-IB scheme to several simple one-dimensional, two-state model systems that mimic a range of non-adiabatic chemical reactions. The model systems are adapted from Tully's previous works^{10,38} with adjusted length scales. The results obtained by RPMD-IB are compared to those from the exact quantum mechanical theory by solving the time-dependent Schrödinger equation in Eq. (5) for model systems. The simulations based on conventional Ehrenfest dynamics and FSSH are also performed for comparison. For simplicity, the mass of the quantum particle is chosen to be 2000 a.u. (atomic units will be used throughout this paper). The system is initially prepared in the lower energy state at 50 K, where the de Broglie wavelength becomes comparable to that of the model systems under study, making nuclear quantum effects non-negligible. It also represents the physical temperature at

which the thermal and quantum fluctuations of the system need to be taken into account in RPMD simulations. Thanks to the presence of complex interatomic potentials in real materials, this represents a physical temperature with both thermal and quantum distributions of nuclei at this particular temperature taken into account.

In the model calculation, the RPMD-IB employs 200 beads in the propagation of the ring polymer system, and the number of beads is referenced from Tully's previous work for convergence.³⁸ The centroid of all beads is initially located at $R_0 = -3 a_0$ with the velocity $v_0 = 0.006$ a.u., where a_0 is the Bohr radius. The real-time electronic population is obtained by averaging the population of all beads in each state. For the Ehrenfest and FSSH dynamics, all trajectories are of the same R_0 and v_0 as the ring polymer centroid initially. We use 2000 trajectories in the FSSH calculations, and the electronic population on each state is equal to the proportion of all trajectories at the corresponding level. The classical mechanical equations of motion for the particle are integrated numerically using the velocity Verlet algorithm.

In the exact quantum mechanical solutions, the quantum wavepacket of the particle is propagated by the Crank–Nicholson method, and the initial wavepacket is chosen to be in Gaussian form,

$$\chi(R, t=0) = A \exp(ik(R - R_0)) \exp(-\alpha(R - R_0)^2), \quad (27)$$

where A is the normalization constant and $\alpha = 0.53$, making the full width at half maxima (FWHM) of the wavepacket equal to the size of the ring polymer system, and the distribution of all beads resembles the wavepacket-determined probability. Momentum k is equal to 12 a.u., mimicking the motion of a classical particle in Ehrenfest and FSSH dynamics. The time-dependent Schrödinger equations for the wavepacket are solved in the diabatic representation and converted to the adiabatic representation for comparison with Ehrenfest, FSSH, and RPMD-IB approaches. We employed an integration time step of 1 a.u. throughout our calculations.

A. Simple avoided crossing

The simple avoided crossing model is defined in the diabatic representation,

$$\begin{aligned} V_{11} &= A(1 - e^{-BR}), R \geq 0, \\ V_{11} &= -A(1 - e^{BR}), R < 0, \\ V_{22} &= -V_{11}, \\ V_{12} &= V_{21} = Ce^{-DR^2}, \end{aligned} \quad (28)$$

where $A = 10^{-2}$, $B = 4$, $C = 5 \times 10^{-3}$, $D = 6.25$. V_{11} and V_{22} are the diabatic potential energy. V_{12} and V_{21} are the coupling terms. The adiabatic potential energy and non-adiabatic coupling strength can be obtained by diagonalizing the diabatic potential matrix and computed by Eq. (8), which are shown in Fig. 2(a).

The time evolution of the electronic population on the excited state using different methods is shown in Fig. 3. Both Ehrenfest dynamics and FSSH methods give similar numerical results but significantly deviate from the exact quantum theory. Due to the classical particle approximation, the population described by Ehrenfest and FSSH stays at zero until the nucleus enters the non-adiabatic

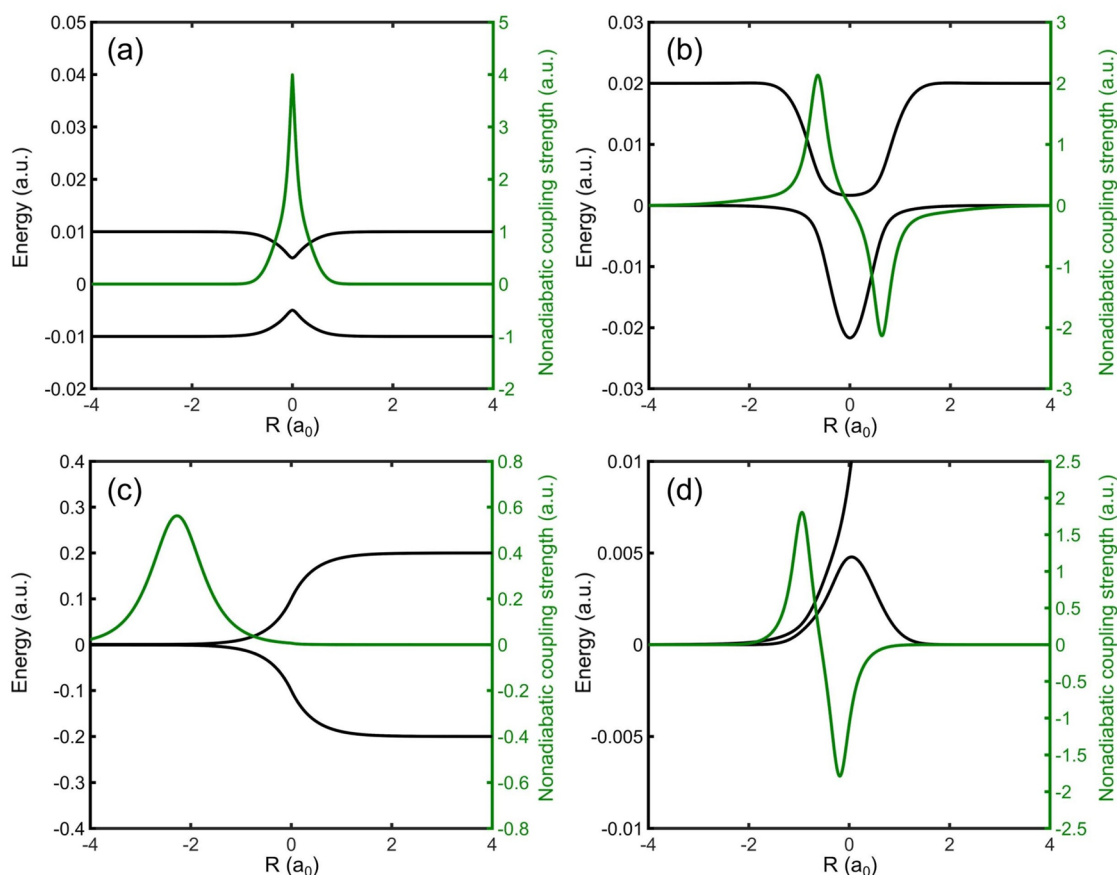


FIG. 2. Adiabatic potential energy curves (solid lines) and the non-adiabatic coupling strength (green lines) for four two-level model systems considered here. (a) Simple avoided crossing. (b) Dual avoided crossing. (c) Extended coupling with reflection. (d) Repulsive potential.

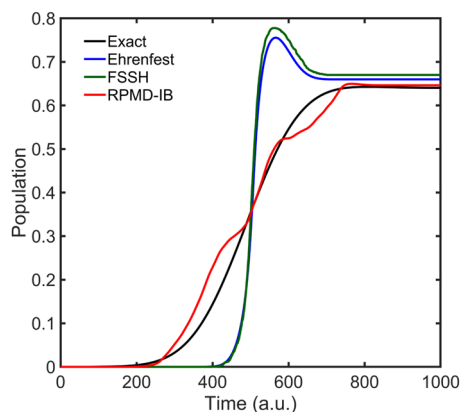


FIG. 3. Real-time population on the excited state obtained from four methods in the simple avoided crossing model, including exact quantum wave packet dynamics (black line), Ehrenfest dynamics (blue line), FSSH (green line), and RPMD-IB (red line).

region near $t = 400$ a.u. when it shows a sharp increase. The population is slightly higher than the exact result after the nucleus leaves the non-adiabatic region.

As for RPMD-IB and exact quantum dynamics, the population increases at an earlier time around $t = 200$ a.u. compared to Ehrenfest and FSSH simulations because the quantized nucleus with a broadened spatial distribution would enter the non-adiabatic region earlier than the classical particle. Therefore, the electronic transition is accelerated due to the nuclear quantum effect. The RPMD-IB approach shows an excellent agreement with the exact solution during the dynamical process, no matter whether the nucleus is in or out of the strong NAC region.

To further demonstrate the stability of the IB approach, we keep the two adiabatic potential curves unchanged but significantly increase the NAC strength to five and ten times the original value, respectively. The results are shown in Fig. 4.

When the NAC strength increases, the population obtained from Ehrenfest and FSSH methods shows significant oscillations in the non-adiabatic region. The oscillation frequency also increases with the NAC strength, leading to a large deviation from the exact

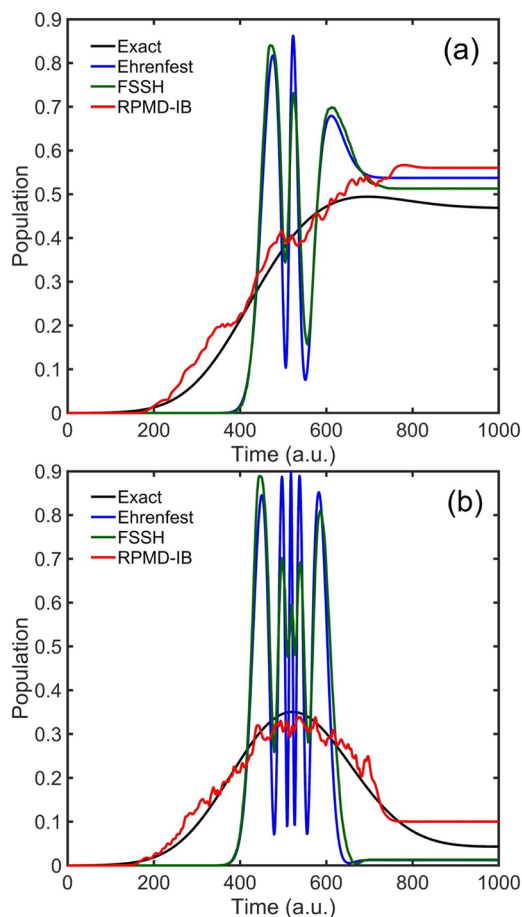


FIG. 4. Real-time population obtained from exact quantum wave packet dynamics (black line), Ehrenfest dynamics (blue line), FSSH (green line), and RPMD-IB (red line) when changing the non-adiabatic coupling strength. (a) The non-adiabatic coupling strength is five times the original strength. (b) The non-adiabatic coupling strength is ten times the original strength.

evolution. This oscillation arises from the excessive NAC strength. When $d_{ij}(R) \gg E_i(R)$, the first term on the rhs of Eq. (10) can be neglected, and then, Eq. (10) can be further approximated to

$$\ddot{c}_2 = -|\dot{R} \cdot d_{12}(R)|^2 c_2 \quad (29)$$

in this two-state model system. Therefore, coefficient c_2 executes a harmonic motion under the excessive NAC strength, with the angular frequency $\Omega = |\dot{R} \cdot d_{12}(R)|$. We also simulate the evolution of population via Eq. (29) using the same NAC strength shown in Fig. 4(b). The result is shown in Fig. 5. Five peaks are also reproduced during the time propagation using Eq. (29) in the time range from 400 to 600 a.u., in good agreement with the simulation result in Fig. 4(b).

Although the RPMD-IB approach employs the mean-field effective potential for each bead, the population averaged over the constituent 200 beads in the ring polymer still shows a good agreement with the exact results shown in Fig. 4 since the quantum nature

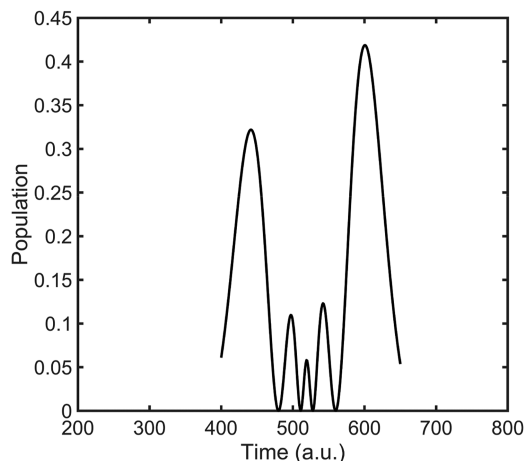


FIG. 5. The approximated evolution of excited state population using Eq. (29) when the non-adiabatic coupling strength is ten times the original strength.

of the nuclear spatial distribution is considered in the RPMD-IB approach. While in the Ehrenfest and FSSH methods, inadequate results are given in the strong NAC region.

Besides changing the NAC strength, we also modify the energy gap between the two states, as shown in Fig. 6. The real-time population on the excited state is shown in Fig. 7.

The electronic population on the excited state decreases as the energy gap increases. When the excited population is large, as shown in Figs. 7(a)–7(c), RPMD-IB shows good agreement with the exact results, while Ehrenfest and FSSH simulations exhibit certain differences from the full quantum dynamics. On the other hand, when the excited population is small, as shown in Fig. 7(d), the RPMD-IB slightly overestimates the population after the nucleus leaves the strong NAC region, while the FSSH can give the final population closest to the exact population in this case.

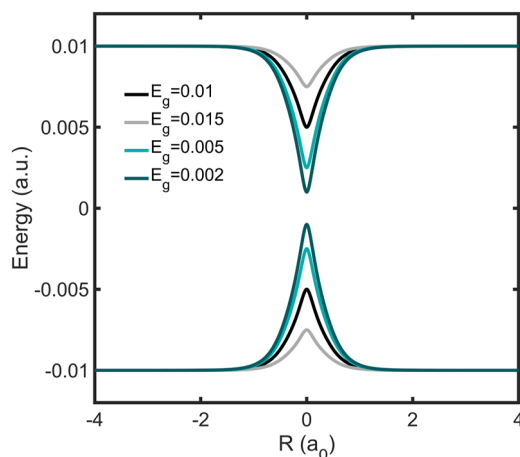


FIG. 6. The adiabatic potential energy surfaces after changing the energy gap.

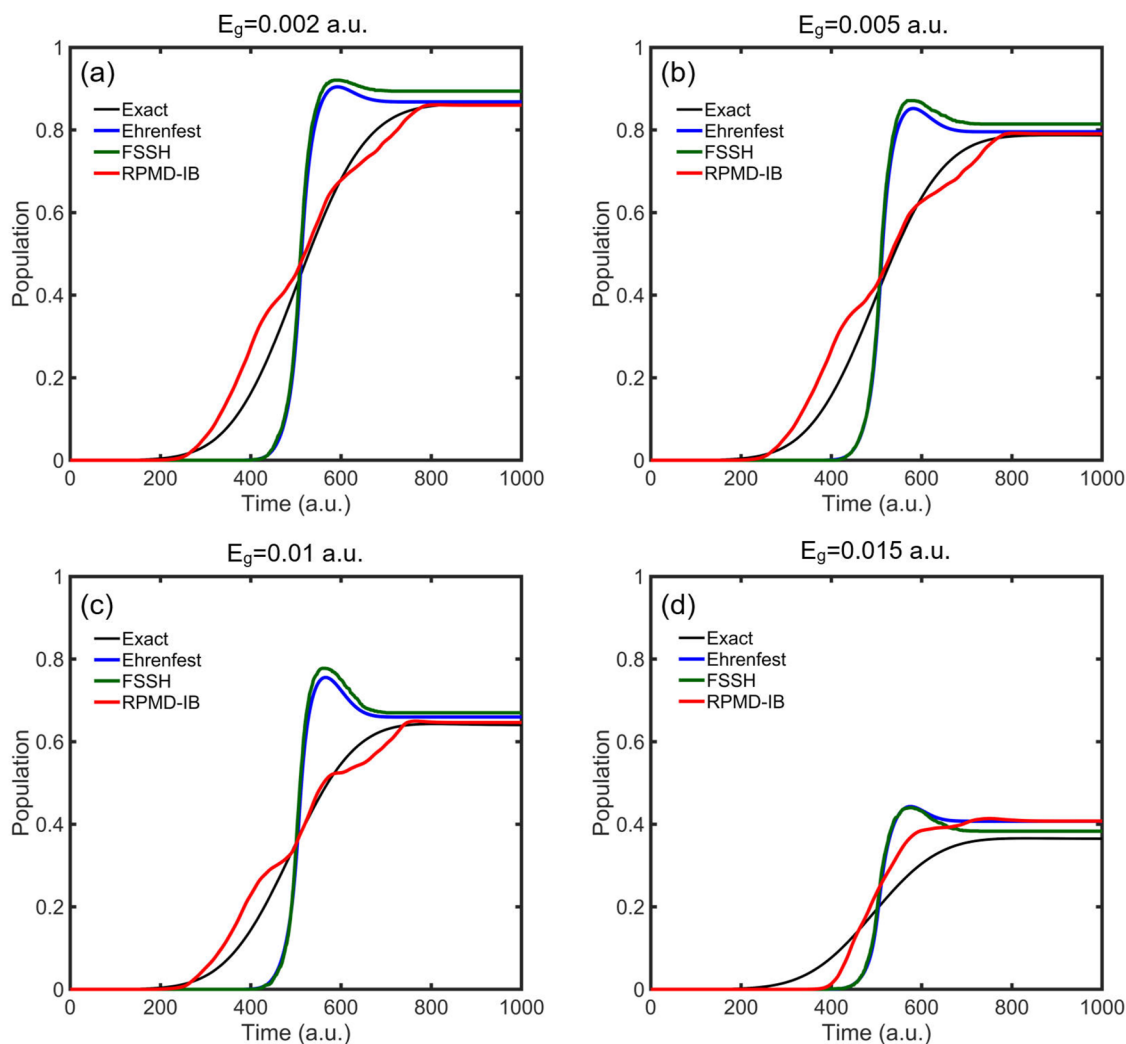


FIG. 7. The real-time excited state population for the cases with the same non-adiabatic coupling strength but different energy gaps. (a) $E_g = 0.002$ a.u., (b) $E_g = 0.005$ a.u., (c) $E_g = 0.01$ a.u., and (d) $E_g = 0.015$ a.u.

B. Dual avoided crossing

The second two-level model exhibits two avoided crossings in the potential energy surfaces. The interactions in the diabatic representation are

$$\begin{aligned} V_{11} &= 0, \\ V_{22} &= A - Be^{-CR^2}, \\ V_{12} &= V_{21} = De^{-ER^2}, \end{aligned} \quad (30)$$

with parameters chosen to be $A = 2 \times 10^{-2}$, $B = 4 \times 10^{-2}$, $C = 1.75$, $D = 6 \times 10^{-3}$, $E = 3.75 \times 10^{-1}$. The adiabatic PESs and NAC strength are shown in Fig. 2(b).

The real-time electronic population on the excited state is shown in Fig. 8.

Similar to the results of the simple avoided crossing model, the excited state population begins to increase near $t = 300$ a.u. for Ehrenfest and FSSH methods due to the classical particle approximation. However, the quantized nucleus with a broad spatial distribution would enter the non-adiabatic region earlier than the classical nucleus. The evolution of excited state population, therefore, begins to increase near an earlier time $t = 100$ a.u. and shows good agreement with the exact results.

C. Extended coupling with reflection

The potential energies of the extended coupling with reflection model in the diabatic representation are

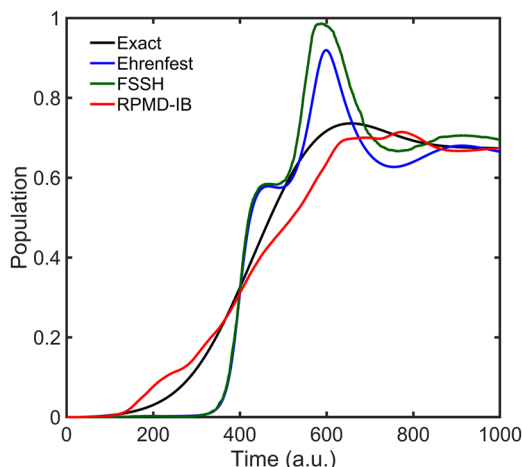


FIG. 8. Real-time population on the excited state obtained from the four methods in the dual avoided crossing model, including exact quantum wave packet dynamics (black line), Ehrenfest dynamics (blue line), FSSH (green line), and RPMD-IB (red line).

$$\begin{aligned} V_{11} &= 6 \times 10^{-4}, \\ V_{22} &= -V_{11}, \\ V_{12} &= A - Be^{-CR}, R \geq 0, \\ V_{12} &= Be^{CR}, R < 0, \\ V_{21} &= V_{12}, \end{aligned} \quad (31)$$

with the parameters chosen to be $A = 2 \times 10^{-1}$, $B = 10^{-1}$, $C = 2.25$. The adiabatic potential energy surfaces and non-adiabatic coupling are shown in Fig. 2(c). This model is difficult to deal with in the Born–Oppenheimer approximation because there exists an energy

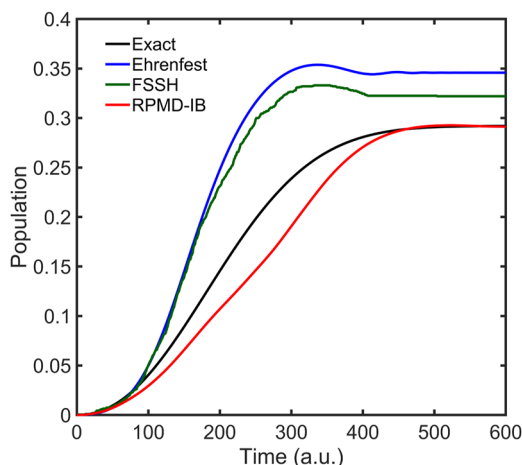


FIG. 9. Real-time population on the excited state obtained from the four methods for the extended coupling with the reflection model, including the exact quantum wave packet dynamics (black line), Ehrenfest dynamics (blue line), FSSH (green line), and RPMD-IB (red line).

barrier in the excited state. The nucleus can simply propagate forward moving on the lower energy state but would be reflected by the barrier in the higher energy state because the kinetic energy here is not enough to cross this barrier.

The real-time population of the excited state is shown in Fig. 9. Contrary to the results in the simple avoided crossing model and dual avoided crossing model, the population obtained by FSSH is smaller than that by the Ehrenfest dynamics because the kinetic energy of the particle is lower than the barrier, and the rejected hops would happen. The RPMD-IB approach shows excellent agreement with the exact results, as compared to the dynamics from Ehrenfest and FSSH schemes.

To further identify the differences between the Ehrenfest dynamics and FSSH simulations, we also compare the nuclear trajectories obtained by these two methods with the exact wavepacket distribution. The results are shown in Fig. 10. The trajectory obtained by the Ehrenfest dynamics is shown [blue line in Fig. 10(a)]. When the nucleus leaves the NAC region, it is accelerated and moves forward. The mean-field potential is a downward effective energy surface because the electronic population on the excited state is less than the ground state. However, a part of the wavepacket is reflected

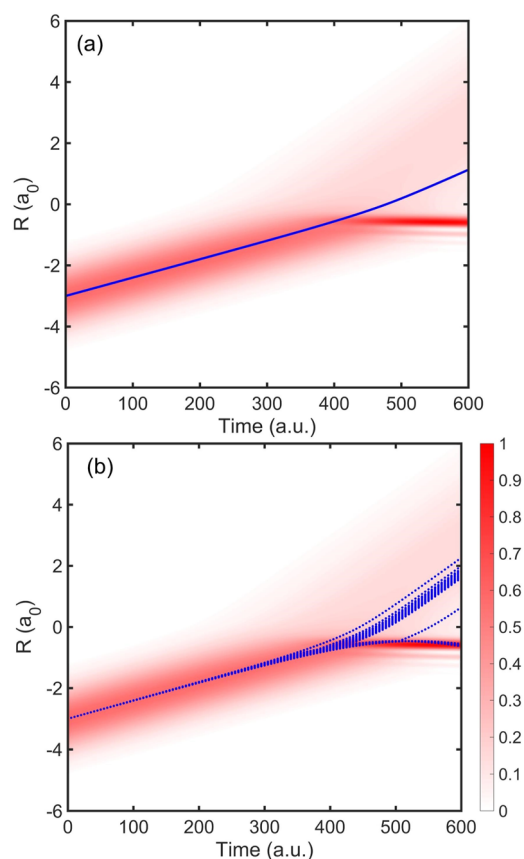


FIG. 10. Comparison of the trajectories obtained by (a) Ehrenfest dynamics (solid line) along with the (b) FSSH method (dashed line) and probability distribution of the nuclear wave function obtained by the wavepacket dynamics (red contour map).

as demonstrated in the red contour map, which cannot be reproduced by the Ehrenfest dynamics since only a single trajectory is considered.

In the FSSH scheme, as shown in Fig. 10(b), a part of the trajectories move forward on the lower energy state, and the other trajectories are reflected by the upper energy level when hitting the barrier, which is in good agreement with the wavepacket splitting behavior in the exact quantum dynamics. However, the spatial distribution of the classical trajectories in FSSH simulations is much narrower compared to the full quantum wavepacket distribution.

The trajectory distribution obtained from the RPMD-IB approach is shown in Fig. 11 when the ring polymer leaves the NAC region. Part of the beads are reflected by the repulsive potential, and the rest beads go across the energy barrier, which is similar to the wavepacket propagation. Although the distribution does not perfectly match the distribution from the exact quantum theory, the splitting is well reproduced in the RPMD-IB approach.

D. Repulsive potential

The last model problem is defined by the following interactions in the diabatic representation:

$$\begin{aligned} V_{11} &= Ae^{-BR^2}, \\ V_{22} &= Ce^{2E(R-D)} + 2Ce^{E(R-D)}, \\ V_{12} &= V_{21} = Fe^{-GR^2}. \end{aligned} \quad (32)$$

The choices of parameters used for the calculation are $A = 5 \times 10^{-3}$, $B = 2$, $C = 10^{-5}$, $D = -2.8$, $E = 1.2$, $G = 2$. The adiabatic potentials and NAC coupling strength are shown in Fig. 2(d). The ground state has a small energy barrier that the nucleus can easily cross, but the potential energy increases exponentially with the nuclear coordinate, and the nucleus would be reflected by this excited state potential.

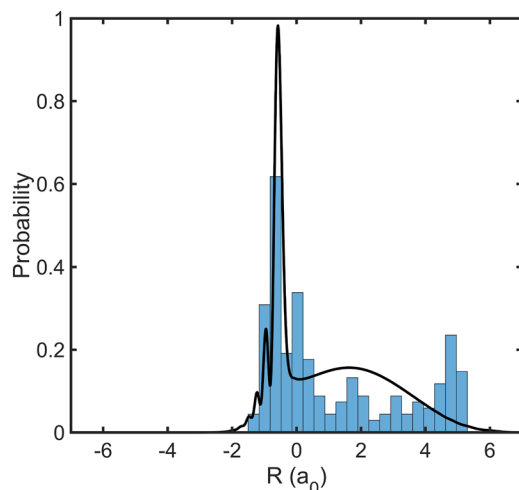


FIG. 11. Comparison between the spatial distribution of beads (blue bars) and the nuclear wavepacket probability integrated over electronic degrees of freedom (black line) after the particle leaves the non-adiabatic coupling region ($t = 530$ a.u.).

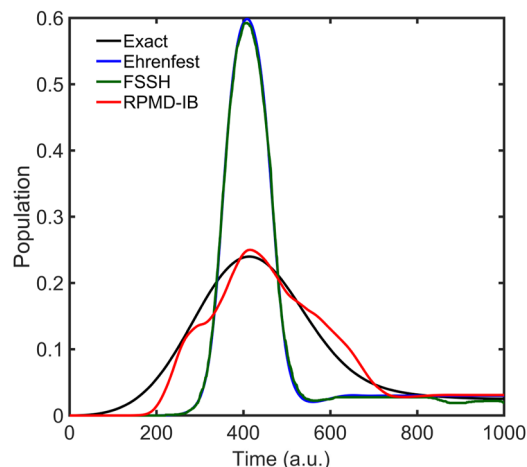


FIG. 12. Real-time population on the excited state obtained from four methods in the repulsive potential model, including exact quantum wave packet dynamics (black line), Ehrenfest dynamics (blue line), FSSH (green line), and RPMD-IB approaches (red line).

The electronic evolution is shown in Fig. 12. Both the Ehrenfest and FSSH methods show results similar to each other, and they both significantly overestimate the highest population during the quantum transition process, as compared to the results from the exact theory. Excellent agreements between the RPMD-IB approach and the exact full quantum dynamics are found, no matter whether the nucleus is in or out of the strong NAC region. The RPMD-IB method developed in this work still provides a consistent improvement over commonly adopted mixed quantum-classical molecular dynamics.

VI. DISCUSSION

We have presented an efficient approach for carrying out molecular dynamics simulations in systems where non-adiabatic electronic transition effects and nuclear quantum effects are both considered. This approach is practical and can be applied in situations involving a large number of nuclei and electrons. The RPMD-IB approach extends the conventional RPMD approach to the non-adiabatic situations where electronic transitions occur, driven by nuclear motions. It also extends the classical nuclear dynamics of the Ehrenfest scheme to the quantum regime under the assumption that each bead in the isomorphic ring polymer resides on an independent mean-field potential energy surface. The electronic configurations are evaluated separately for each bead at a given time, and the ring polymer motion is governed by the isomorphic Hamiltonian derived in Eq. (23). This independent-bead approximation is tested against the exact quantum mechanical calculations for several one-dimensional, two-state model systems, along with the results obtained from the conventional mixed quantum-classical simulation schemes, such as Ehrenfest and FSSH approaches. In these model systems, we find that the proposed RPMD-IB scheme provides excellent agreement with the exact quantum mechanical results, while the Ehrenfest and FSSH schemes would give

inadequate results in some situations, especially when the nucleus is in the strong non-adiabatic coupling region.

In fact, the performances of Ehrenfest and FSSH approaches based on a single classical initial trajectory can be significantly improved when considering a quantum distribution of nuclear trajectories. However, in practice simulations of real materials, the conventional Ehrenfest dynamics within the framework of real time TDDFT often employs a single trajectory instead of multiple trajectories with an initial condition distribution. The FSSH scheme widely used for real materials adopts the classical path approximation to combine with TDDFT,^{51,52} which also follows the single trajectory strategy. In such cases, the RPMD-IB approach significantly improves the accuracy of dynamic simulations compared to conventional FSSH and Ehrenfest dynamics by incorporating quantum distributions of nuclei. The RPMD-IB scheme differs from multiple-trajectory Ehrenfest and FSSH dynamics in that the quantum distribution of trajectory and nuclear quantum effects, such as quantum tunneling and zero-point energy, are included, while they are missing in the latter two schemes, which sample a thermalized Boltzmann initial distribution. Although, in principle, multiple-trajectory Ehrenfest and FSSH schemes can also start from a quantum (Wigner) distribution of nuclei, the quantum distribution therein has to be preset beforehand, while RPMD-IB naturally samples the nuclear quantum distribution of a given PES based on path integral techniques.

The alternative nonadiabatic RPMD methods, such as NRPM, CS-RPMD, and SM-NRPM, are explicit in theory and might have some advantages over RPMD-IB. For example, the RPMD-IB approach still inherits some problems of standard Ehrenfest dynamics, such as the absence of detailed balance. However, the mapping formalism remains challenging to combine with first-principles TDDFT-based algorithms for simulation of realistic molecules and materials. The proposed RPMD-IB is shown to be a reliable scheme for the models presented in this work. In addition, it can be easily combined with TDDFT. A more efficient nonadiabatic RPMD algorithm with the TDDFT framework requires further investigation.

We employed 200 beads in the model calculation for convergence, which induces extra computational complexity. The implementation of a parallel computing strategy employing one bead per computer node can significantly reduce computational time costs. Remarkably, this strategy could achieve a comparable computational efficiency to standard Ehrenfest dynamics in large systems.

The distribution of beads from the RPMD-IB approach does not perfectly match the exact evolution of wavepacket distribution from quantum mechanics. For instance, RPMD-IB does not reproduce well wavepacket splitting in dynamical quantum transition processes. The population evolution is also sensitive to the initial bead configuration and requires the distribution resembling the initial wavepacket distribution ([supplementary material](#)). In addition, the RPMD-IB approach does inherit some deficiencies in conventional adiabatic RPMD, such as the spurious frequencies in spectra calculations due to the artifacts caused by the harmonic interaction in the ring polymer isomorphism. These artifacts could potentially be stronger in a multi-surface method, such as RPMD-IB, where different polymer beads can potentially experience very different Ehrenfest forces. This problem may be solved with proper thermostats in further studies. The explicit treatment of electronic

decoherence is also absent in the evolution of the electronic subsystem. However, this problem is relieved since in a ring polymer isomorphism, each individual bead follows its own separate path and the amplitude for electronic configurations is evaluated separately. Therefore, the spreading of paths will naturally lead to a loss of phase coherence when averaging the results of all beads.

VII. SUMMARY

In summary, based on the tests in Sec. V, the RPMD-IB approach proposed here is a promising scheme to approximate full quantum simulations of molecules and materials. The models examined here exhibit strong quantum behaviors, and the RPMD-IB approach gives encouraging agreements with the exact full quantum dynamics, indicating that this scheme successfully incorporates the nuclear quantum effects in the non-adiabatic simulations. In general, we believe that the RPMD-IB approach is applicable to more complex, realistic multidimensional material when electronic transitions and nuclear quantum effects play an important role.

SUPPLEMENTARY MATERIAL

The final population probability using different initial bead configurations and numbers of beads is provided in the [supplementary material](#). In addition, the population probability vs final momentum in different model systems is also included. See the [supplementary material](#) for evolution with different initial conditions and other results.

ACKNOWLEDGMENTS

We acknowledge partial financial support from the National Natural Science Foundation of China (Grant Nos. 12025407, 12404293, 12450401, and 92250303), the National Key Research and Development Program of China (Grant No. 2021YFA1400201), and the Chinese Academy of Sciences (Grant Nos. XDB330301 and YSBR047).

AUTHOR DECLARATIONS

Conflict of Interest

The authors have no conflicts to disclose.

Author Contributions

Ruji Zhao: Conceptualization (equal); Data curation (equal); Formal analysis (equal); Funding acquisition (equal); Investigation (equal); Methodology (equal); Project administration (equal); Resources (equal); Software (equal); Supervision (equal); Validation (equal); Writing – original draft (equal); Writing – review & editing (equal). **Sheng Meng:** Conceptualization (equal); Data curation (equal); Formal analysis (equal); Funding acquisition (equal); Investigation (equal); Methodology (equal); Project administration (equal); Resources (equal); Software (equal); Supervision (equal); Validation (equal); Writing – original draft (equal); Writing – review & editing (equal).

DATA AVAILABILITY

The data that support the findings of this study are available from the corresponding author upon reasonable request.

REFERENCES

- ¹M. Born and R. Oppenheimer, *Ann. Phys.* **389**, 457 (1927).
²J. C. Tully, *Modern Methods for Multidimensional Dynamics Computations in Chemistry* (World Scientific, 1998), p. 34.
³J. C. Tully, *J. Chem. Phys.* **137**, 22A301 (2012).
⁴M. P. Bircher *et al.*, *Struct. Dyn.* **4**, 061510 (2018).
⁵J. C. Tully, *Faraday Discuss.* **110**, 407 (1998).
⁶R. Kapral and G. Ciccotti, *J. Chem. Phys.* **110**, 8919 (1999).
⁷R. Kapral, *Annu. Rev. Phys. Chem.* **57**, 129 (2006).
⁸R. Crespo-Otero and M. Barbatti, *Chem. Rev.* **118**, 7026 (2018).
⁹P. Ehrenfest, *Z. Phys.* **45**, 455 (1927).
¹⁰J. C. Tully, *J. Chem. Phys.* **93**, 1061 (1990).
¹¹N.-K. Chen, X.-B. Li, J. Bang, X.-P. Wang, D. Han, D. West, S. Zhang, and H.-B. Sun, *Phys. Rev. Lett.* **120**, 185701 (2018).
¹²M.-X. Guan, E. Wang, P.-W. You, J.-T. Sun, and S. Meng, *Nat. Commun.* **12**, 1885 (2021).
¹³S. Hammes-Schiffer and J. C. Tully, *J. Chem. Phys.* **101**, 4657 (1994).
¹⁴D. Borgis and J. T. Hynes, *J. Phys. Chem.* **100**, 1118 (1996).
¹⁵U. Müller and G. Stock, *J. Chem. Phys.* **107**, 6230 (1997).
¹⁶F. J. Webster, J. Schnitker, M. S. Friedrichs, R. A. Friesner, and P. J. Rossky, *Phys. Rev. Lett.* **66**, 3172 (1991).
¹⁷M. H. Beck, A. Jäckle, G. A. Worth, and H.-D. Meyer, *Phys. Rep.* **324**, 1 (2000).
¹⁸H. D. Meyer, U. Manthe, and L. S. Cederbaum, *Chem. Phys. Lett.* **165**, 73 (1990).
¹⁹G. W. Richings, I. Polyak, K. E. Spinlove, G. A. Worth, I. Burghardt, and B. Lasorne, *Int. Rev. Phys. Chem.* **34**, 269 (2015).
²⁰A. Abedi, N. T. Maitra, and E. K. U. Gross, *J. Chem. Phys.* **137**, 22A530 (2012).
²¹A. Abedi, N. T. Maitra, and E. K. U. Gross, *Phys. Rev. Lett.* **105**, 123002 (2010).
²²D. Marx and M. Parrinello, *J. Chem. Phys.* **104**, 4077 (1996).
²³M. Parrinello and A. Rahman, *J. Chem. Phys.* **80**, 860 (1984).
²⁴R. P. Feynman, A. R. Hibbs, and D. F. Styer, *Quantum Mechanics and Path Integrals* (Courier Corporation, 2010).
²⁵B. J. Berne and D. Thirumalai, *Annu. Rev. Phys. Chem.* **37**, 401 (1986).
²⁶T. E. Markland and M. Ceriotti, *Nat. Rev. Chem.* **2**, 0109 (2018).
²⁷J. Cao and G. A. Voth, *J. Chem. Phys.* **100**, 5106 (1994).
²⁸J. Cao and G. A. Voth, *J. Chem. Phys.* **100**, 5093 (1994).
²⁹J. Cao and G. A. Voth, *J. Chem. Phys.* **101**, 6157 (1994).
³⁰I. R. Craig and D. E. Manolopoulos, *J. Chem. Phys.* **121**, 3368 (2004).
³¹S. Habershon, D. E. Manolopoulos, T. E. Markland, and T. F. Miller III, *Annu. Rev. Phys. Chem.* **64**, 387 (2013).
³²K. A. Müller and H. Burkard, *Phys. Rev. B* **19**, 3593 (1979).
³³E. Fallacara, P. Depondt, S. Huppert, M. Ceotto, and F. Finocchi, *J. Phys. Chem. C* **125**, 22328 (2021).
³⁴P. Loubeyre, F. Occelli, and P. Dumas, *Nature* **577**, 631 (2020).
³⁵L. Monacelli, I. Errea, M. Calandra, and F. Mauri, *Nat. Phys.* **17**, 63 (2021).
³⁶J. Chen, X.-Z. Li, Q. Zhang, M. I. J. Probert, C. J. Pickard, R. J. Needs, A. Michaelides, and E. Wang, *Nat. Commun.* **4**, 2064 (2013).
³⁷I. Silvera, *Proc. Natl. Acad. Sci. U. S. A.* **107**, 12743 (2010).
³⁸P. Shushkov, R. Li, and J. C. Tully, *J. Chem. Phys.* **137**, 22A549 (2012).
³⁹X. Tao, P. Shushkov, and T. F. Miller III, *J. Chem. Phys.* **148**, 102327 (2017).
⁴⁰J. O. Richardson and M. Thoss, *J. Chem. Phys.* **139**, 031102 (2013).
⁴¹S. N. Chowdhury and P. Huo, *J. Chem. Phys.* **147**, 214109 (2017).
⁴²D. Bossion, S. N. Chowdhury, and P. Huo, *J. Chem. Phys.* **154**, 184106 (2021).
⁴³A. Mandal, S. S. Yamijala, and P. Huo, *J. Chem. Theory Comput.* **14**, 1828 (2018).
⁴⁴W. Zhou, A. Mandal, and P. Huo, *J. Phys. Chem. Lett.* **10**, 7062 (2019).
⁴⁵R. Zhao, P. You, and S. Meng, *Phys. Rev. Lett.* **130**, 166401 (2023).
⁴⁶M. Born, K. Huang, and M. Lax, *Am. J. Phys.* **23**, 474 (1955).
⁴⁷R. B. Gerber, V. Buch, and M. A. Ratner, *J. Chem. Phys.* **77**, 3022 (1982).
⁴⁸T. J. Hele, *arXiv:1308.3950* (2013).
⁴⁹J. R. Schmidt and J. C. Tully, *J. Chem. Phys.* **127**, 094103 (2007).
⁵⁰C. D. Schwieters and G. A. Voth, *J. Chem. Phys.* **111**, 2869 (1999).
⁵¹A. V. Akimov and O. V. Prezhdo, *J. Chem. Theory Comput.* **9**, 4959 (2013).
⁵²A. V. Akimov and O. V. Prezhdo, *J. Chem. Theory Comput.* **10**, 789 (2014).